AN ABSTRACT OF THE THESIS OF

Marsha C. Lampi for the degree of Honors Baccalaureate of Science in Bioengineering presented on May 31st, 2012. Title: Molecular origins of peptide entrapment within polyethylene oxide brush layers.

Abstract approved:

_____

Dr. Joseph McGuire

Effective surface coatings for tissue-contacting medical devices should prevent both biofilm formation and infection. One method to achieve this aim is protein repellant polyethylene oxide (PEO) brush coatings loaded with antimicrobials. Previous research has demonstrated that the antimicrobial nisin adsorbs to PEO brush layers in multi-layer amounts and suggests that small peptides or proteins are capable of being loaded into an otherwise protein repellent brush. The work described in this thesis aimed to understand the influences of peptide structure and amphiphilicity on adsorption into brush layers and is a necessary step in the development of bioactive coatings. Optical waveguide lightmode spectroscopy was used to investigate the adsorption of polyglutamic acid and the cationic amphiphilic peptide WLBU2 to a PEO brush. Kinetic parameters were interpreted with respect to a model accounting for history-dependent adsorption, in order to evaluate rate constants for peptide adsorption and desorption, as well as the lateral clustering behavior of an absorbed or entrapped peptide. The WLBU2 peptide was held within the brush even after sustained rinsing, whereas the desorption data suggested that polyglutamic acid would completely elute from the brush with time. These results indicate that small peptides are capable of becoming entrapped within PEO brushes and that amphiphilic peptides are held more tightly. The results presented here are compelling evidence of the potential to create anti-fouling surface coatings capable of storing and delivering therapeutics.

Key Words: PEO brush layer, OWLS, WLBU2

Molecular origins of peptide entrapment within polyethylene oxide brush layers

by

Marsha C. Lampi

A PROJECT

submitted to

Oregon State University

University Honors College

in partial fulfillment of

the requirements for the

degree of

Honors Baccalaureate of Science in Bioengineering (Honors Scholar)

Presented May 31, 2012

Commencement June 2012

Honors Baccalaureate of Science in Bioengineering project of Marsha C. Lampi presented on May 31, 2012.

APPROVED:

Mentor, representing Chemical, Biological, and Environmental Engineering

---

Committee Member, representing Chemical, Biological, and Environmental Engineering

---

Committee Member, representing Chemical, Biological, and Environmental Engineering

---

Head, School of Chemical, Biological, and Environmental Engineering

---

Dean, University Honors College

I understand that my project will become part of the permanent collection of Oregon State University, University Honors College. My signature below authorizes release of my project to any reader upon request.

Marsha C. Lampi, Author

ACKNOWLEDGEMENTS

I am extremely thankful for the guidance provided by my mentor, Dr. Joe McGuire, to complete this project, as well as his contributions to my professional development as a bioengineer. I would also like to thank Dr. Karl Schilke for his expertise and assistance in all experimental matters. This project would not be possible without the contributions of the entire McGuire Lab Team, and relied on collaboration with Justen Dill, Kain Wu, and Matt Ryder. I would also like to acknowledge the University Honors College for generously awarding me the Honors Promise Finishing Scholarship to support this work.

TABLE OF CONTENTS

LIST OF FIGURES

LIST OF FIGURES (continued)

LIST OF TABLES

LIST OF APPENDIX FIGURES

LIST OF APPENDIX FIGURES (continued)

Molecular origins of peptide entrapment within polyethylene oxide brush layers

Introduction

Need for biocompatible device coatings

Protein adsorption and biofilm formation is a major concern in the development of medical devices that come into contact with human tissue. Patient health is at risk due to a decrease in device functionality caused directly by fouling, as well as thrombosis and bacterial infections that may occur as a consequence of biofilm formation. Treatments for surface-induced infections are costly and often require surgery to replace the device, systemic antibiotic administration, and long hospital stays. Of increasing concern are deadly, multi-drug resistant pathogens that do not respond to current antibiotic treatments.[1] An ideal biocompatible surface coating would protect patients by preventing protein adsorption and delivering therapeutics to suppress infection.

Protein adsorption at surfaces

Protein adsorption driven by energetic and entropic effects is readily observed when solid surfaces are contacted by protein containing solutions. Time dependent conformational changes in protein structure occur as proteins unfold and form non-covalent contacts with a surface. It is well established that protein adsorption becomes increasingly irreversible as time progresses due to the formation of these contacts, and an optimal protein-surface equilibrium is reached, *Figure 1*.[1]

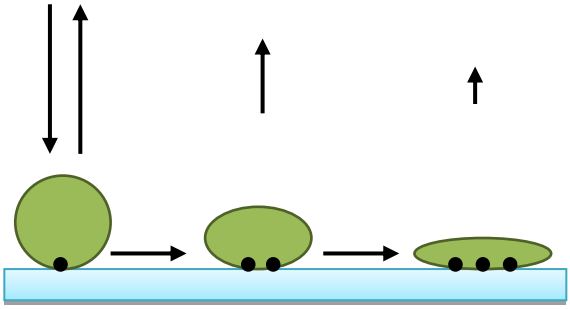

Figure 1: Protein unfolding results in conformational changes. An increasing number of non-covalent contacts between the surface and protein slows desorption until it becomes irreversible with time.[1]

Adsorption kinetics are unique for each system based on the individual protein present, the solvent, and the surface characteristics. A simple Langmurian model can be used for the primary adsorption of protein onto a bare surface. In this case, the rate of adsorption $\left(\frac{d\Gamma}{dt}\right)$ is affected by system specific adsorption (k_a) and desorption (k_d) constants, the bulk adsorbate concentration (c_b), and the area available for adsorption $\left(1-\hat{a}'\Gamma\right)$, where $\hat{a}'$ represents the area occupied by each molecule, *Equation 1*.

$$\frac{d\Gamma}{dt} = k_a c_b \left(1-\hat{a}'\Gamma\right) - k_d\Gamma \tag{1}$$

History dependent protein adsorption has been observed when a surface is cyclically exposed to protein-containing and protein-free solutions. The kinetics of adsorption at later times depend on both the surface area available, the structure of previously adsorbed proteins, and interactions between incoming molecules and those already adsorbed on the surface. A faster rate of adsorption at equal levels of adsorbed mass has been observed for various protein-surface systems, *Figure 2*.[2-4]

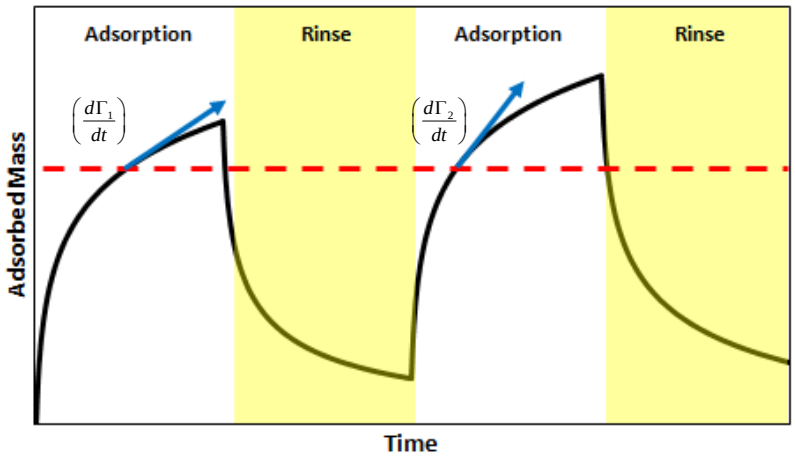

Figure 2: A schematic of a typical history dependent protein adsorption pattern. During the second adsorption, $\left(\frac{d\Gamma}{dt}\right)$ is greater than the previous cycle when the net adsorbed mass at the dashed line is equal.

The observed increase in adsorption rate at equal levels of adsorbed mass can be attributed to lateral protein clustering along the surface creating a larger cavity space, Φ, that is readily available for protein adsorption, *Figure 3*.[2,4]

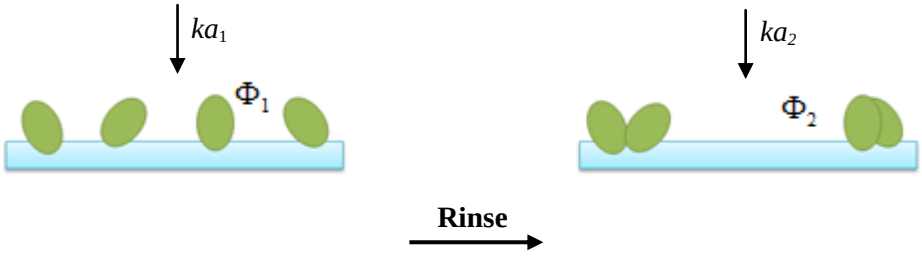

Figure 3: Lateral protein clustering along a surface creates a greater accessible area for protein adsorption even when the net adsorbed mass is conserved, $k_{a2} > k_{a1}$ and $\Phi_2 > \Phi_1$.

PEO surface coatings and protein repelling abilities

Polyethylene oxide (PEO) is widely recognized as a hydrophilic polymer that inhibits protein adsorption to surfaces via elastic and osmotic repulsive forces.[5] At sufficiently high grafting densities, such that the radii of individual PEO chains overlap and are forced away from a surface, a brush layer is formed. In a brush, PEO protein repulsion capabilities are independent of chain length, and strong protein repulsion has been reported for brush layers containing just two ethylene oxide units.[1,3] As a protein approaches a PEO brush surface the polymer chains are compressed resulting in an elastic repulsive fore. A second repulsive force is generated when chain compression removes hydrating water molecules and creates a thermodynamically unfavorable osmotic pressure.[1] Adsorption will only occur if the effective interactive potential, $U_{eff}(z)$, between a protein and the brush layer is energetically favorable. The attraction to the uncoated surface, $U_{bare}(z)$ would have to overcome the repulsive forces of the brush, $U_{brush}(z)$, and is function of *z*, the distance from the surface, *Equation 2*.[6]

$$U_{eff}(z) = U_{bare}(z) + U_{brush}(z) \tag{2}$$

It has been hypothesized that below the hydrophilic outer region of the PEO brush, a hydrophobic core capable of binding proteins may exist. This core would be attractive for the adsorption of proteins that are sufficiently small to enter the PEO layer.[6,7]

PEO brush layers can be synthesized through self-assembled monolayers (SAMs) of co-polymer tri-blocks containing a hydrophobic center-block flanked by PEO pendant chains. When an aqueous solution of tri-blocks is placed in contact with a hydrophobic surface, the hydrophobic center-block will preferentially locate at the surface with the PEO chains extended into solution, *Figure 4*.[8]

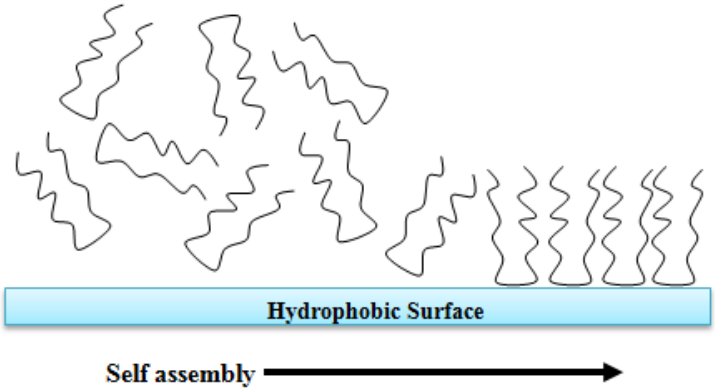

Figure 4: Brush layer self-assembly occurs through hydrophobic associations between the tri-block center-block and the surface in aqueous solution.

Pluronic® F108 is an FDA approved PEO-PPO-PEO ((polyethylene-oxide)-(polypropylene-oxide)-(polyethylene oxide)) tri-block that is known to form protein repellent brush layers through spontaneous self-assembly. The initial brush layer is stabilized by hydrophobic association between the PPO center-block and the surface, however, it can be permanently immobilized to derivatized surfaces using gamma irradiation to form covalent bonds.[3,8]

Antimicrobial properties of WLBU2

WLBU2 is a synthetic 24-residue cationic antimicrobial peptide (RRWVRRVRRWVRRVVRVVRRWVRR) that was engineered to overcome the limitations of current antibiotics against multi-drug resistant pathogens As a class, cationic peptides are believed to work by assuming secondary (alpha helix, beta sheet) or tertiary structures with opposing hydrophobic and hydrophilic regions within the apolar environment of the cell membrane. The amphiphilic structure enables the peptides to successfully cross or disrupt both Gram-positive and Gram-negative bacterial membranes leading to cell death.[9,10]

The WLBU2 sequence was derived from the lentivirus lytic peptide 1 (LLP_1) found on the C-terminus end of the HIV-1 virus. LLP_1 is a transmembrane protein that was found to be a potent antimicrobial and is believed to contribute to HIV pathogenicity. The amino acid sequence

for WLBU2 was selected such that the location of arginine, valine, and tryptophan residues create hydrophobic and hydrophilic faces when an alpha helix structure is assumed in membrane mimetic conditions. In an aqueous environment, WLBU2 is disordered, *Figure 5*.

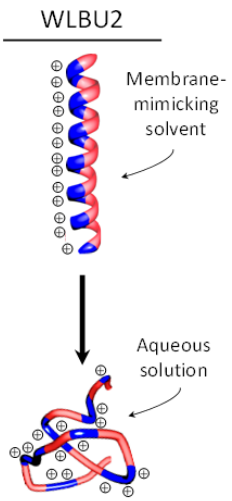

Figure 5: WLBU2 is an amphiphilic cationic peptide. In a solvent mimicking the apolar environment of the cell-membrane its structure is an alpha helix with hydrophilic and hydrophobic faces. WLBU2 is disordered in aqueous soltution.

Ariginine and valine amino acids were selected to increase the peptide cationicity and hydrophobicity, respectively. Tryptophan was included to increase peptide activity in cell membranes and to augment its overall potency. The optimal length for the WLBU2 peptide was determined experimentally.[9] The viability of WLBU2 as a potent antimicrobial has been proven based on its efficacy against a broad range of bacteria, fungi, and parasites as well as its activity in both human serum and whole blood.[10,11]

Nisin adsorption into PEO brush layers

Nisin is a 3.4 kDa amphiphilic peptide that effectively inhibits Gram-positive bacteria by destabilizing the bacterial membrane. Although brush layers are widely used for their protein repelling capabilities, it has been shown that nisin is able to adsorb in multi-layer quantities into

F108 brushes. Nisin association within the brush is believed to occur as a result of entrapment by extended pendant PEO chains rather than primary adsorption to the underlying surface below. It is significant to note that nisin maintains its antimicrobial activity after associating with the brush and that nisin loaded F108 brushes maintain their ability to repel protein as evidenced by fibrinogen challenges.[12,13] The adsorption of nisin indicates the potential of creating therapeutic loaded brush layers.

Polyglutamic acid and polylysine as model peptides

Polyglutamic acid and polylysine are polymers of a single amino acid whose secondary structure can be tightly controlled between alpha helix and disordered conformations based on solution conditions. Above its isoelectric point (pH 3.0) polyglutamic acid contains a negative charge and assumes a disordered structure. Below its isoelectric point, polyglutamic acid is neutral and its structure is an alpha helix.[14] Polylysine is positively charged below its isoelectric point (pH 11.4) taking on a disordered conformation, and becomes an alpha helix when it is neutral and above it, *Figure 6*.[15]

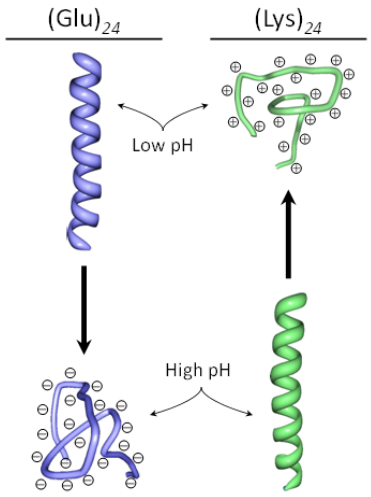

Figure 6: Polyglutamic acid and polylysine are model peptides whose structure can be controlled between disordered and alpha helix conformations based on solution pH.

Statement of Purpose

There is an extensive literature record concerning the protein repellent properties of PEO brush layers, and the mechanism of repulsion continues to be a topic of investigation. On the other hand, the adsorption of peptides and proteins into PEO brush layers has scarcely been reported despite the important clinical significance to create bioactive coatings capable of storing and delivering therapeutics. This study aimed to begin to understand the molecular origins of peptide entrapment within PEO brush layers.

Multilayer adsorption of nisin into PEO brushes was reported by Tai et al. The observed adsorption pattern was indicative of nisin entrapment within the PEO pendant chains rather than primary adsorption at the surface; however, the mechanism is not fully understood.[12] It is hypothesized that both peptide structure and amphiphilicity influence the peptide-PEO interactions that lead to entrapment.

This research aimed to understand the mechanism of peptide entrapment within PEO brush layers using model peptides whose structure and amphiphilicity could be tightly controlled. The adsorption to PEO layers by polyglutamic acid and WLBU2 was investigated. Future research will also focus on polylysine as a model peptide, but experimental challenges prevented discernible results from being obtained.

Materials and Methods

Introduction to materials and methods

Optical waveguide lightmode spectroscopy (OWLS) was used to study peptide adsorption to F108 brush layers. Silica dioxide (SiO_2) coated waveguides were treated with trichlorovinylsilane (TCVS) using established methods to create a uniform hydrophobic surface through the addition of silane groups. F108 brush layers were then formed through self-assembly and the propensity of the tri-block center-block to preferentially locate at the surface due to hydrophobic associations. The brush layer was permanently immobilized at the surface using gamma radiation to form covalent bonds.

The effects of structure and amphiphilicity on peptide adsorption to the F108 modified waveguides were investigated using polyglutamic acid and WLBU2 as model peptides. Hydrophobic TCVS treated waveguides were used as control surfaces. The structure of polyglutamic acid was controlled between disordered and helix conformations by varying solution pH. WLBU2 served as an amphiphilic peptide and has a disordered conformation in aqueous solution. Adsorption challenges to the brush layers were performed using adsorption-rinse cycles. OWLS data were also recorded using polylysine as well as polyglutamic acid on unmodified silica. Reasonable, reproducible results were not observed for polylysine; therefore, further testing with the peptide was not pursued.

Optical waveguide lightmode spectroscopy

OWLS is a method to study protein adsorption kinetics in real-time based on changes in refractive index. Silica substrates coated with a $Si_{0.25}Ti_{0.75}O_2$ waveguide embossed layer are used as sensors, *Figure 7*. [15]

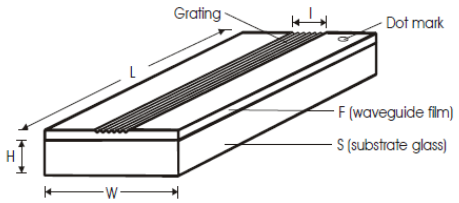

Figure 7: Schematic of an OWLS waveguide sensor.[15]

The sensors used in this project were coated with a second ~10 nm uniform SiO_2 coating. OWLS analysis relies on the incoupling of linearly polarized light from a Ne-He (632.8 nm) laser. The OWLS stage containing the sensor is rotated between -5 and 5º from horizontal while the laser position is fixed to locate the incoupling angles corresponding to the transverse electric and transverse magnetic waves. The incoupling angle is sensitive to surface changes (i.e. adsorption) altering the refractive index of the evanescent field directly above the waveguide. Adsorbed mass at the surface can be calculated using system software as a function of the incoupling angle and the refractive index, *Figures 8*.[15,16]

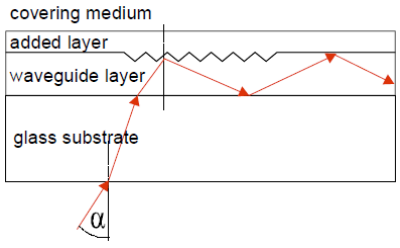

Figure 8: Adsorbed mass at the sensor surface is calculated based on refractive index and a change in the angle of incident light (α) needed to produce an incoupling effect within the waveguide grating.[16]

Preparation of F108 modified waveguides

Silanization, as reported by McPherson et al. effectively creates a hydrophobic priming layer for self-assembled PEO brush layers using trichlorovinylsilane (TCVS). TCVS reacts with the silica surface to produce HCl gas and obtain a free hydroxyl group. Hydrogen bonding between vinyl silane and surface hydroxyls then occurs. After curing with heat, the surface contains vinyl groups that serve as the hydrophobic layer, *Figure 9*.[17]

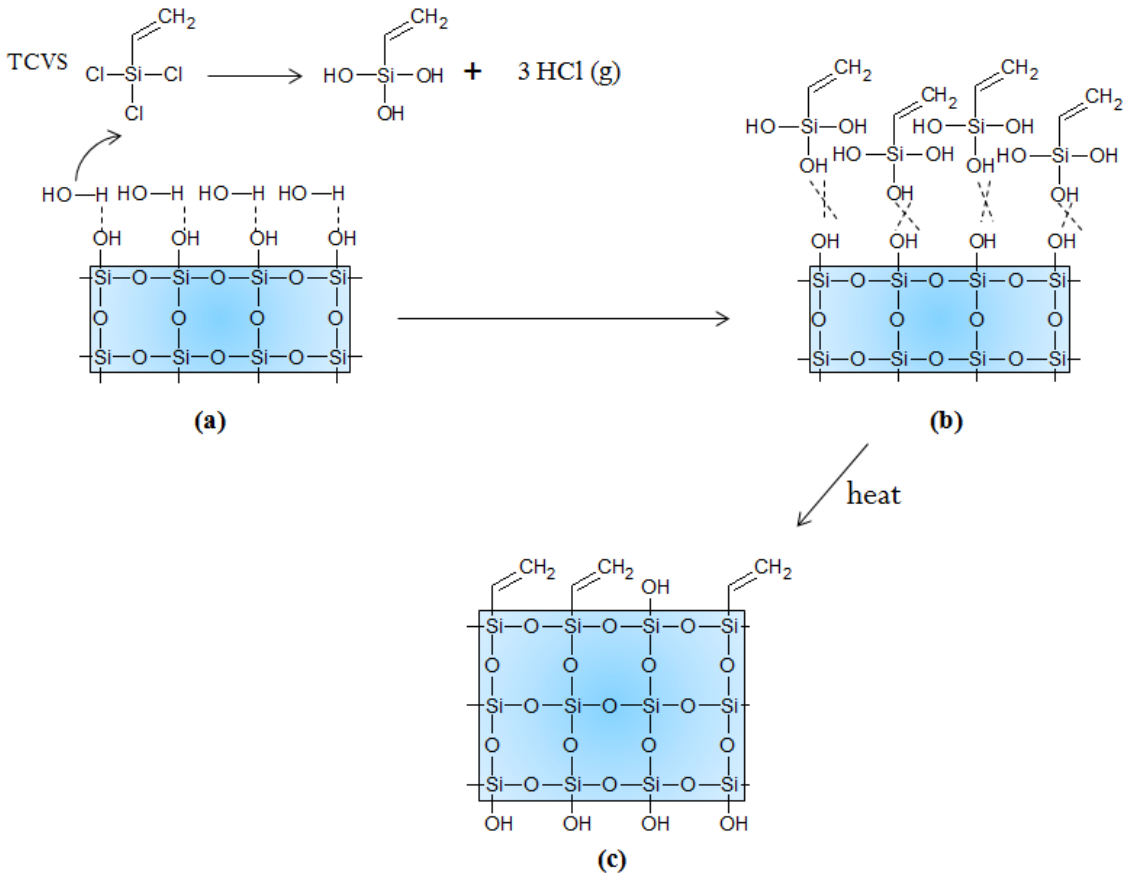

Figure 9: Schematic of TCVS chemistry on silica surfaces. TCVS reacts with the surface to produce HCl gas and gain a hydroxyl group (a). Hydrogen bonding ensues (b) and after curing with heat, hydrophobic vinyl groups are present on the surface. *Schematic courtesy of Justen K. Dill.*

OWLS waveguide sensor chips with a ~10 nm surface silica (SiO_2) thin film coating were purchased (MicroVacuum Ltd). In preparation for silanization, the sensors were cleaned by immersing in chromosulfuric acid (ACROS Organics) for 10 minutes at room temperature and

dried with nitrogen gas. An AFM analysis characterizing the chromosulfuric acid cleaning method can be found in the *Appendix*. After cleaning, the sensors were immersed in sieve dried ethanol and dried with nitrogen to remove moisture that could result in surface polymerization. Silanization was performed by chemical vapor deposition at room temperature using an organosilane carrier gas assisted reactor (OSCAR).

The sensors were placed in the sealed reaction chamber with the waveguide surface facing up. Argon gas was used for 20 minutes to purge the system, creating an environment completely devoid of moisture. 0.2 mL of TCVS (TCI America) was then injected into the system, vaporized, and delivered to the waveguide surfaces using the argon carrier gas. After 1 hour of vapor deposition, a second 0.2 mL of TCVS was injected into the system and again allowed to react for 1 hour. The waveguides were then removed from OCSAR and cured at 150 ºC for 1 hour.

Self-assembled F108 brush layers were formed on the silanized waveguide surfaces by incubating overnight with 5% Pluronic® F108 (BASF) in HEPES (GIBCO BRL), pH 7.4. The brush layers were then gamma irradiated at 0.3 Mrad to covalently attach the brush layer to the surface.[15] The PEO functionlized OWLS sensors were dried with N_2 gas and stored away from light. Hydrophobic control sensors that were silanized but not modified with a PEO brush were treated in a similar manner.

Experimental outline

The adsorption of polyglutamic acid and WLBU2 to F108 brush layers on silica waveguides were compared. TCVS silanized silica sensors were used as hydrophobic control surfaces. An outline of the testing performed with each peptide is presented in *Table 1*. WLBU2 adsorption as an alpha helix was not tested due to the complications of developing a membrane mimetic solvent suitable for our system. Testing of polylysine in NaOH and HCl was initially pursued, but abandoned after repeated attempts to obtain reasonable results failed.

Table 1: Experimental outline of OWLS testing with polyglutamic acid and WLBU2 peptides.

	TCVS Silanized Silica	**F108 Brush Layer**
Polyglutamic Acid Disordered	X	X
Polyglutamic Acid Helical	---	X
WLBU2 Disordered	X	X

Peptide preparation

Lyophilized 20-residue average, 3.0 kDa molecular weight poly(L-glutamic acid sodium salt) (Alamanda Polymers, 13.9% Na salt) was purchased and dissolved at 1.0 mg/mL in HPLC water. The polyglutamic acid was separated into 1.0 mL aliquots that were frozen and thawed prior to each experiment. The 1.0 mg/mL poyglutamic acid was diluted to 0.1 mg/mL for OWLS testing in either 1.0 N HCl (EMD Chemicals) or a dilute HCl aqueous solution, pH 4.7 to invoke either helical or disordered conformations, respectively. Lyophilized WLBU2 was synthesized and acquired from GenScript. It was dissolved at 5.0 mg/mL in HPLC water and frozen in 200 μL aliquots. It was thawed and diluted to 0.1 mg/mL in 10 mM PBS, 150 mM NaCl, pH 7.4 for testing. The 0.1 mg/mL peptide solutions were degassed for 40 minutes using a vacuum pump system (Welch Dry Vacuum Pump) immediately prior to all OWLS testing.

Peptide structure was evaluated by circular dichroism (CD) analysis. WLBU2 in PBS showed slight evidence of an alpha helix structure, perhaps due to shielding effects by the sodium salt. Polyglutamic acid suggested evidence of a left-handed helix at both high and low pHs. However, CD spectra for small peptides are not well established; therefore, based on theory, it is still believed polyglutamic acid at a low pH is structurally more ordered than polyglutamic acid at a higher pH.

OWLS testing

Buffer solutions were prepared to match the composition of the 0.1 mg/mL peptide solutions and degassed for 5 hours using the vacuum pump system. The helical polyglutamic acid buffer was 0.9 N HCl to account for dissolving the peptide in HPLC water prior to diluting to 0.1 mg/mL in 1.0 N HCl. Based on similar reasoning, the disordered buffer was prepared by adding 10% HPLC water to the HCl solution used to dissolve the peptide. In the case of WLBU2, the buffer was simply 10 mM PBS, 150 mM NaCl, pH 7.4 due to the concentrated peptide aliquots.

Waveguide sensors were equilibrated overnight in the appropriate buffer and the refractive index of the HCl solutions were calculated using linear interpolation of the values obtained by Olsen.[18] At the start of each run, a sensor was loaded into OWLS and allowed to equilibrate within the system for 40-60 minutes. OWLS Relative Intensity Mode (RIM) with buffer introduced at 50.0 μL/min (OWLS^{TM} 210-SIS) was used. When the baseline slopes were on the order of $1.0 \cdot 10^{-9}$, ~4 mL of 0.1 mg/mL peptide solution was introduced into the system and adsorption to the sensor was allowed to occur for 30 minutes. Adsorption was followed by a 30 min rinse where peptide-free buffer was introduced. The adsorption-rinse cycle was then repeated. At the conclusion of each test, the OWLS system was cleaned with HPLC water and 0.1 N HCl.

Data Analysis

Overview of analysis

Adsorbed mass vs. time data was obtained from OWLS, and the adsorption patterns were used to make qualitative conclusions. Kinetic rates constants and the cavity function were calculated based on a mass balance where the rate of adsorption, $\frac{d\Gamma}{dt}$, is affected by the intrinsic adsorption constant, k_a, the bulk concentration of the adsorbing species, c_b, the fractional surface area available for adsorption, Φ, the desorption rate constants for each adsorbed state, k_{di}, and the amount of adsorbed mass in each state, Γ_i, *Equation 3*.

$$\frac{d\Gamma}{dt} = k_a c_b \Phi - \sum_i k_{d,i} \Gamma_i \tag{3}$$

The rate constants and cavity function were used to elucidate how the polyglutamic acid and WLBU2 peptides interacted with and adsorbed to the F108 brush layers.

Adsorption rate constant and the cavity function

The intrinsic rate of adsorption, is commonly presented with an exponential term accounting for the energy barrier to adsorption, $e^{-\frac{f(\Gamma)}{RT}}$ and was used in our model, *Equation 4*.

$$\frac{d\Gamma}{dt} = k_a e^{-\frac{f(\Gamma)}{RT}} c_b \Phi - \sum_i k_{d,i} \Gamma_i \tag{4}$$

The value of the k_a term is unknown, except at the single point in each system where Γ=0, therefore, k_a can be more fully described as a k_a' term evaluated at Γ=0, *Equation 5*.

$$k_a' = k_a e^{-\frac{f(\Gamma|_{\Gamma=0})}{RT}} \tag{5}$$

Substitution of k_a' into *Equation 4* necessitates division by $e^{-\frac{f(\Gamma|_{\Gamma=0})}{RT}}$ to keep the original equation unaltered and rearrangement results in *Equation 6*.

$$\frac{d\Gamma}{dt} = k_a' c_b \frac{e^{-\frac{f(\Gamma)}{RT}}}{e^{-\frac{f(\Gamma|_{\Gamma=0})}{RT}}} \Phi - \sum_i k_{d,i} \Gamma_i \tag{6}$$

The cavity function, Φ, represents the probability of finding free area on the surface where adsorption can occur, and accounts for slower rates of adsorption occurring when less area is available. In the simplest model based on hard core repulsive forces, the cavity function is the fraction of the surface where a molecule can adsorb without overlapping a molecule already on the surface. A modified cavity function, Φ' can be used to account for the attractive and repulsive forces that must be overcome for adsorption to occur. With respect to *Equation 5*, Φ' is a grouping of the activation energies necessary for adsorption, *Equation* 7.

$$\Phi' = \frac{e^{-\frac{f(\Gamma)}{RT}}}{e^{-\frac{f(\Gamma|_{\Gamma=0})}{RT}}} \Phi \tag{7}$$

A revised mass balance accounting for the energy barriers of adsorption is presented in *Equation 8*.

$$\frac{d\Gamma}{dt} = k_a' c_b \Phi' - \sum_i k_{d,i} \Gamma_i \tag{8}$$

The adsorption rate constant for each system was calculated as a combined term, "$k_a' c_b$" which incorporates the intrinsic rate of adsorption and the adsorbate bulk concentration. The $k_a' c_b$ term was obtained by generating a plot of $\frac{d\Gamma}{dt}$ vs. Γ and performing a linear regression on the surface-limited adsorption regime where *Equation 8* is valid, *Figure 10*.

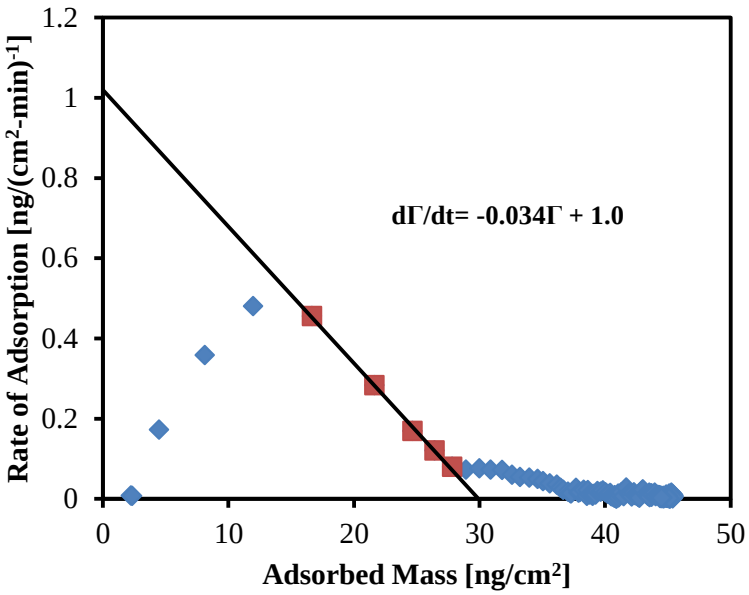

Figure 10: Representative plot of disordered WLBU2 adsorption to the F108 brush illustrating the method used to identify the combined adsorption constant, $k_a' c_b$. $k_a' c_b$ is the y-intercept when adsorbed mass at the surface equals zero.

Extrapolation of the line to a bare surface (Γ =0) causes the desorption rate constants to drop out and Φ =1, such that the y-intercept is $k_a' c_b$, *Equation 9.*

$$\left.\frac{d\Gamma}{dt}\right|_{\Gamma=0} = k_a' c_b \tag{9}$$

$k_a' c_b$ was assumed to be constant for each experiment because by definition k_a' is an intrinsic property of the peptide within the system. Bulk peptide concentration was assumed to be constant as the peptide adsorbing to the surface was negligible in terms of the total peptide in solution. [2]

The modified cavity function can be calculated by solving *Equation 8.* In particular, the cavity function can be calculated at the beginning of the second adsorption cycle where it is assumed all the adsorbed peptide after rinsing is irreversibly bound State 3 peptide. At equal levels of adsorbed mass during the first cycle, it is being assumed all the adsorbed peptide is also irreversibly bound because this initial population was the first to contact the surface and undergo

surface-induced conformational changes. Based on these assumptions, the desorption term of *Equation 8* is eliminated. The modified cavity function, can be easily solved by rearrangement of *Equation 8* as a function of the adsorption rate, $\frac{d\Gamma}{dt}$ and the combined adsorption constant, $k_a' c_b$ for the system, *Equation 10.*[2]

$$\Phi' = \frac{\left(\frac{d\Gamma}{dt}\right)}{k_a' c_b} \tag{10}$$

The cavity function is used to identify lateral clustering movement of peptides along a surface (or within the brush). Values for the cavity function where $\Phi_2 > \Phi_1$ explain increased adsorption rates when the net amount of adsorbed mass on a surface is equal.

Desorption rate constants and peptide populations

A three state system was assumed to obtain the desorption rate constants. State 1 represented peptides that were most loosely bound to the surface and desorbed at the fastest rate, k_{d_1}. State 2 represented peptides that desorbed from the surface at the slowest rate, yet still left the surface at rate k_{d_2}. State 3 represented peptides that had undergone conformational changes irreversibly binding them to the surface such that $k_{d_3} = 0$. The values of k_{d_1} and k_{d_2} were found using the slopes of the desorption plot during the first rinse cycle, $\frac{d\Gamma}{dt}$ vs. Γ (the negative adsorption plot) based on *Equation 2* with the adsorption terms going to zero, *Equation 11*.

$$\frac{d\Gamma}{dt} = \sum_i k_{d,i} \Gamma_i \tag{11}$$

From this plot, two distinct peptide populations and rates of desorption could be identified, with the faster rate at high surface coverages representing State 1 and the lower rate representing State

2. The slopes of the best fit lines representing these populations are k_{d1} and k_{d2}, respectively. The peptide remaining on the surface at the end of a 30 minute rinse was the population in State 3, *Figure 11*.[2]

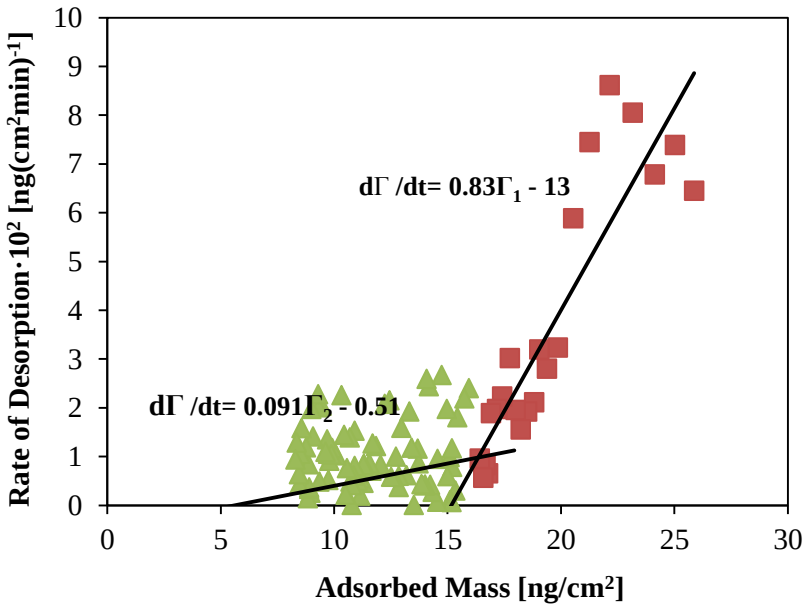

Figure 11: Representative plot of disordered polyglutamic acid desorption from the F108 brush to illustrate the method used to identify the desorption rate constants and populations of State 1, 2, and 3 peptides.

The peptide populations, Γ_1, Γ_2, and Γ_3, were also determined from the desorption vs. adsorbed mass plot (*Figure 11*). The intercept of the two lines is the point at which all Γ_1 peptide has left the surface. The Γ_1 population was calculated using a mass balance subtracting the value of adsorbed mass at the intercept from the amount of peptide adsorbed at the onset of rinsing, *Equation 12.*

$$\Gamma_1 = (\text{Mass at the onset of desorption})-(\text{Mass after } \Gamma_1 \text{ desorption}) \quad (12)$$

The Γ_3 population was then calculated from the State 2 line. The value of the x-intercept is the State 3, irreversibly bound, peptide population when all the State 1 and State 2 peptides have left the surface. Γ_2 was calculated using another mass balance subtracting Γ_1 and Γ_3

from the amount of adsorbed peptide at the onset of rinsing, *Equation 13*.

$$\Gamma_2 = (\text{Mass at the onset of desorption})\text{-}\Gamma_1\text{-}\Gamma_3 \quad (13)$$

In some adsorption data, only a single linear region existed; therefore, it was concluded there was no State 2 peptide.

Results

Polyglutamic acid

Disordered polyglutamic acid in dilute HCl at pH 4.7 was found to adsorb to both the TCVS surface and the F108 brush, *Figure 12*.

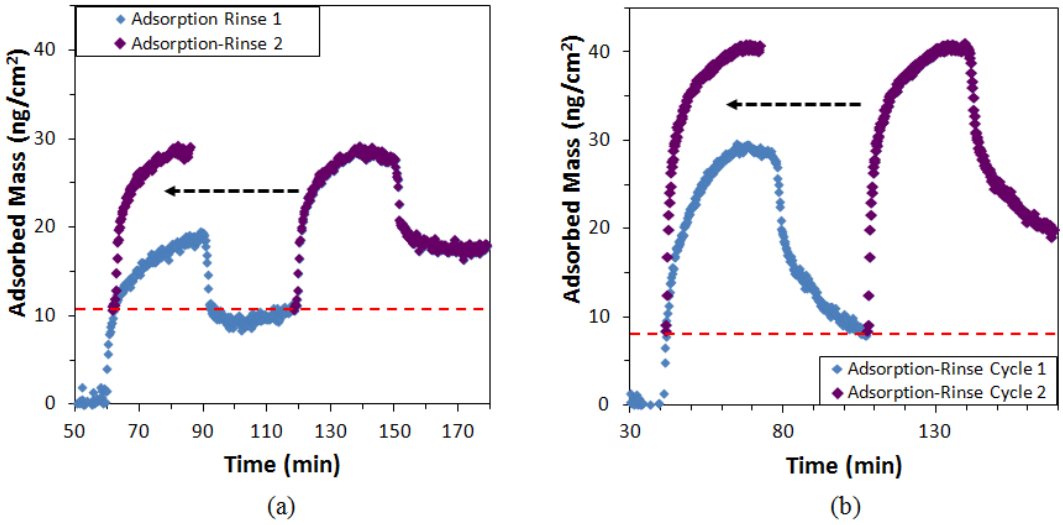

Figure 12: Disordered polyglutamic acid adsorption to a bare TCVS silanized surface (a) and to a F108 brush layer (b). The initial rate of adsorption in the second cycle is shifted backward to compare adsorption rates at equal surface coverages during the first cycle. History dependent adsorption at the dashed line is only present on the bare surface.

Adsorption to the bare surface is lower than to the brush indicating polyglutamic acid does not have a high propensity for adsorption at hydrophobic surfaces. This can be explained by the absence of surface groups on polyglutamic acid capable of forming hydrophobic associations. Adsorption to the F108 brush can be attributed to entrapment by the pendant PEO chains, and the absence of a desorption plateau in *Figure 9b* suggests all the polyglutamic acid would eventually elute. This desorption pattern is also explained by the peptide's non-amphiphilic character as it is unable to form the hydrophobic associations with brush core needed for prolonged retention. History dependent adsorption within the PEO brush is not observed, perhaps indicating the

method of entrapment prevents lateral clustering, or that the peptide is adsorbed in such low amounts that peptide-peptide interactions are not occurring.

No appreciable adsorption to the F108 brush layer by the helical polyglutamic acid in 1.0 N HCl was observed, *Figure 13*.

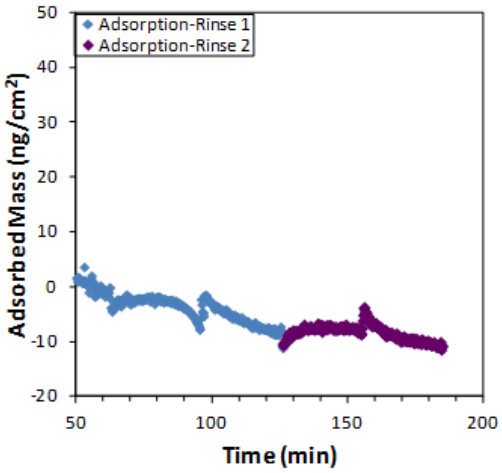

Figure 13: The helical form of polyglutamic acid did not show any appreciable adsorption to the PEO brush. A slight negative baseline shift is present.

Based on the adsorption of the larger more disordered form of the peptide, the absence of adsorption is unlikely. Instead, it possibly indicates that the more ordered polyglutamic acid was able to freely exchange without becoming entrapped such that adsorption and desorption occurred at similar rates. As suggested by the desorption pattern in *Figure 9b*, once incorporated within the brush layer, there are no associations to immobilize a non-amphiphilic peptide for a prolonged amount of time.

WLBU2 adsorption

Disordered WLBU2 in PBS, pH 7.4 was also found to adsorb to both the TCVS surface and the F108 brush, *Figure 14*.

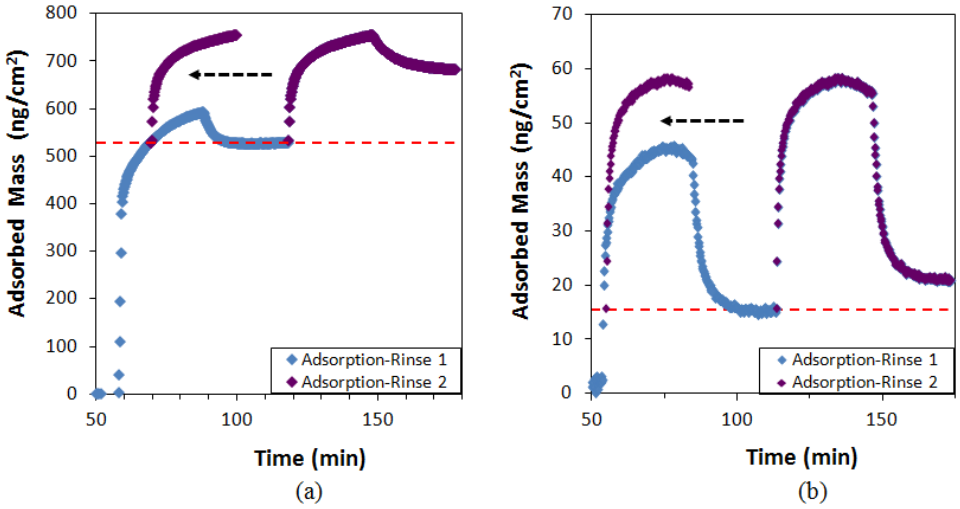

Figure 14: Disordered WLBU2 adsorption to a bare TCVS silanized surface (a) and to a F108 brush layer (b). The high levels of adsorption on the bare surface may be indicative of multi-layer WLBU2 adsorption. The initial rate of adsorption in the second cycle is shifted backward to compare adsorption rates at equal surface coverages during the first cycle. History dependent adsorption is very pronounced on the bare surface.

WBLU2 readily adsorbed to the TCVS surface owing to its partial hydrophobic character. The exceptionally high levels of adsorption may be indicative of multi-layer adsorption. Appreciable adsorption of WLBU2 is also present within the brush, however in much lower amounts compared to the bare surface. The post-rinsing plateau at 15 ng/cm^2 in *Figure 13b* is significant as it indicates WLBU2 can be loaded and retained within brush layers. The retention of WLBU2 is explainable by hydrophobic associations with the PEO brush core that occur as a result of the peptide's amphiphilic character. History dependent adsorption of WLBU2 within the PEO brush is not observed, and can be explained using the same reasoning as for polyglutamic acid.

Figures 12 and 14 both indicate that peptide adsorption to a PEO brush is distinctly different than the behavior observed at a bare surface. These results are significant because they suggest the peptides are adsorbing or becoming entrapped within the PEO brush itself and are not associating with the underlying hydrophobic surface below.

Summary of calculated adsorption parameters

The kinetic parameters for the adsorption of disordered polyglutamic acid and WLBU2 to both TCVS and PEO brush layer surfaces are summarized in *Table 2*.

Table 2: Summary of kinetic parameters for the adsorption to TCVS and PEO brush surfaces by disordered polyglutamic acid and WLBU2 peptides.

	Polyglutamic Acid		**WLBU2**	
	TCVS	**PEO Brush**	**TCVS**	**PEO Brush**
$k_a' c_b$ [ng·(cm^2·min)$^{-1}$]	0.14	0.16	18	1.0
k_{d_1} [min^{-1}]	0.041	0.012	$5.9 \cdot 10^{-3}$	6.9·-3
k_{d_2} [min^{-1}]	---	$6.1 \cdot 10^{-4}$	---	---
k_{d_3} [min^{-1}]	0	0	0	0
Γ_1 [ng/cm^2]	8.1	11	66	25
Γ_2 [ng/cm^2]	---	18	---	---
Γ_3 [ng/cm^2]	11	0.62	530	18
Φ_1 [ ]	0.21	0.61	$5.6 \cdot 10^{-3}$	0.45
Φ_2 [ ]	0.70	0.63	0.11	0.46

The calculated adsorption parameters confirm the conclusions that were made based on the adsorption plots. On the bare surface history dependent adsorption occurs for both peptides as evidenced by $\Phi_2 > \Phi_1$. Adsorption to the PEO brush was <u>not</u> history dependent for either peptide, as $\Phi_2 \approx \Phi_1$. Also of significance is that the adsorption rate constant to the PEO brush is approximately one order of magnitude greater for the amphiphilic WLBU2 peptide than for the

non-amphiphilic polyglutamic acid peptide. The desorption rate constant (k_{d_1}) for the most loosely held peptide population (Γ_1), is one order of magnitude greater for polyglutamic acid than for WLBU2. These parameters indicate that amphiphilic peptides have a higher propensity to adsorb to PEO brush layers, and are held more tightly after adsorbing. The visual conclusion that all the polyglutamic acid would eventually elute from the brush was confirmed by a calculated Γ_3 population of 0.62 ng/cm^2 and further supports that amphiphilicity is important for long-term peptide retention within a PEO brush.

Discussion and Conclusions

The aim of this work was to investigate the molecular origins of peptide entrapment within PEO brush layers with respect to structure and amphiphilicity. The results indicate that small peptides are able to become entrapped within brush layers irrespective of their amphiphilicity. However, amphiphilic peptides are held more tightly; and therefore, hold the most promise for prolonged loading. Contrary to the hypothesis, disordered peptides were able to incorporate into the brush, whereas the adsorption of the more structured polyglutamic acid helical peptide was not observed. This result can possibly be attributed to simultaneous adsorption and desorption and indicates that peptides must be sufficiently small to penetrate the brush layer, but also large enough to ensure they become entrapped. Helical amphiphilic peptides may be capable of adsorbing and remaining within the brush due to hydrophobic interactions, but remains a topic of future investigations.

In addition to studying the adsorption of helical WLBU2 to the brush, the activity of WLBU2 after adsorption, and its maximum loading level should be investigated to enhance the translational potential of this work. Polylysine as a model peptide should also be revisited. In the context of this work, polylysine adsorption could not be achieved even on surfaces where it was predicted based on electrostatic interactions. However, as a positively charged peptide, polylysine could complement and corroborate the data obtained from polyglutamic acid.

This project was a first step in understanding the effects of peptide structure and amphiphilicity on entrapment within PEO brush layers. Nevertheless, the results concerning WLBU2 are particularly exciting as they indicate a potent cationic peptide is capable of being loaded and retained within a PEO brush after rinsing.

Works Cited

[1] Banerjee, Indrani, Ravindra C. Pangule, and Ravi S. Kane. "Antifouling Coatings: Recent Developments in the Design of Surfaces That Prevent Fouling by Proteins, Bacteria, and Marine Organisms." *Advanced Materials* 23.6 (2011): 690-718. Print.

[2] McGuire, J. *Biomaterials & Biointerfaces Class Notes*. Oregon State University. Spring 2011.

[3] Tie, Y. "Protein Adsorption: Kinetics and History Dependence." *Journal of Colloid and Interface Science* 268.1 (2003): 1-11. Print.

[4] Claudio Calonder, Claudio, Yanrong Tie, and Paul R. Van Tassel. "History Dependence of Protein Adsorption Kinetics." *Proceedings of the National Academy of Sciences* 98.19 (2001): 10664-0669. Print.

[5] Desai, Neil P., and Jeffrey A. Hubbell. "Biological Responses to Polyethylene Oxide Modified Polyethylene Terephthalate Surfaces."*Journal of Biomedical Materials Research* 25.7 (1991): 829-43. Print.

[6] Halperin, A. "Polymer Brushes That Resist Adsorption of Model Proteins: Design Parameters." *Langmuir* 15.7 (1999): 2525-533. Print.

[7] Sheth, S. R., and D. Leckband. "Measurements of Attractive Forces between Proteins and End-grafted Poly(ethylene Glycol) Chains."*Proceedings of the National Academy of Sciences* 93 (1997): 8399-404. Print.

[8] Govender, S., E. Jacobs, M. Bredenkamp, and P. Swart. "A Robust Approach to Studying the Adsorption of Pluronic F108 on Nonporous Membranes." *Journal of Colloid and Interface Science* 282.2 (2005): 306-13. Print.

[9] Deslouches, B., S. M. Phadke, V. Lazarevic, M. Cascio, K. Islam, R. C. Montelaro, and T. A. Mietzner. "De Novo Generation of Cationic Antimicrobial Peptides: Influence of Length and Tryptophan Substitution on Antimicrobial Activity." *Antimicrobial Agents and Chemotherapy* 49.1 (2004): 316-22. Print.

[10] McClanahan, J.r., R. Peyyala, R. Mahajan, R.c. Montelaro, K.f. Novak, and D.a. Puleo. "Bioactivity of WLBU2 Peptide Antibiotic in Combination with Bioerodible Polymer."*International Journal of Antimicrobial Agents* 38.6 (2011): 530-33. Print.

[11] Deslouches, B., K. Islam, J. K. Craigo, S. M. Paranjape, R. C. Montelaro, and T. A. Mietzner. "Activity of the De Novo Engineered Antimicrobial Peptide WLBU2 against Pseudomonas Aeruginosa in Human Serum and Whole Blood: Implications for Systemic Applications." *Antimicrobial Agents and Chemotherapy* 49.8 (2005): 3208-216. Print.

[12] Tai, Yuan-Ching, Joseph McGuire, and Jennifer A. Neff. "Nisin Antimicrobial Activity and Structural Characteristics at Hydrophobic Surfaces Coated with the PEO–PPO–PEO Triblock Surfactant Pluronic® F108." *Journal of Colloid and Interface Science*322.1 (2008): 104-11. Print.

[13] Matt P Ryder, Karl F Schilke, Julie A Auxier, Joseph McGuire, JennifeR A Neff. "Nisin adsorption to polyethylene oxide layers and its resistance to elution in the presence of fibrinogen." *J. Colloid Interface Sci. Vol 350, Is 1, Pg 194-199*. Oct 2010.

[13] Inoue, Keiichi, Naoki Baden, and Masahide Terazima. "Diffusion Coefficient and the Secondary Structure of Poly-L-glutamic Acid in Aqueous Solution." *Journal of Physical Chemistry B* 109.47 (2005): 22623-2628. Print.

[14] Moriyama, Rui, Sung Won Choi, Naohiko Shimada, Arihiro Kano, and Atsushi Maruyama. "Abundant Graft Chains Do Not Influence Coil-to-helix but α-to-β Transition of Polylysine Backbone, Resulting in Thermoreversible β-to-α Transition." *Reactive and Functional Polymers* 67.11 (2007): 1381-387. Print.

[15] *OW 2400 Optical Waveguide Grating Coupler Sensor Chip*. Budapest, Hungary: Micro Vacuum, 2012. Print.

[16] *Optical Waveguide Lightmode Spectroscopy System OWLS 210 & Biosense 2.6 Software User's Manual*. Budapest, Hungary: MicroVacuum, 2011. Print.

[17] McPherson, Timothy B., Hong S. Shim, and Kinam Park. "Grafting of PEO to Glass, Nitinol, and Pyrolytic Carbon Surfaces by γ Irradiation." *Journal of Biomedical Materials Research* 38.4 (1997): 289-302. Print.

[18] Olsen, Allen L. "An Interpolation Table for Refractive Index-Normality Relationship for Solutions of Hydrochloric Acid and Sodium Hydroxide." *Journal of the American Chemical Society* 40 (1937): 117-26. Print.

APPENDIX

An AFM analysis of OWLS waveguide cleaning methods

An atomic force microscopy (AFM) analysis was done by Matt Ryder to investigate the current chromosulfuric acid method used to clean OWLS waveguide sensors. The possible etching of the waveguide sensors by NaOH, a potential buffer for polylysine testing, was also studied. The results are summarized in the following series of AFM images, *Figures A1-A16*.

Figures A1 and A2 are images of two separate OWLS waveguide sensors that were treated identically. Of interest is the varied level of quality either between the two sensors or the amount of surface particles present in the samples.

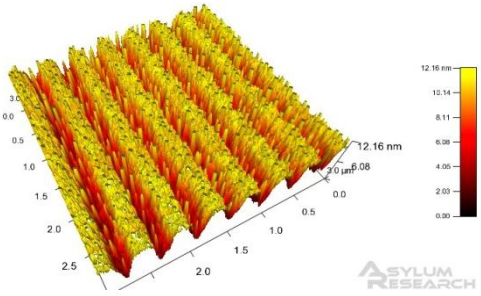

Figure A1: (SiO_2 Waveguide 5109-4) Washed with chromosulfuric acid. Image created on ArGyle Software, and optimized. As seen, 3 x 3 µm by 12.16 nm height range.

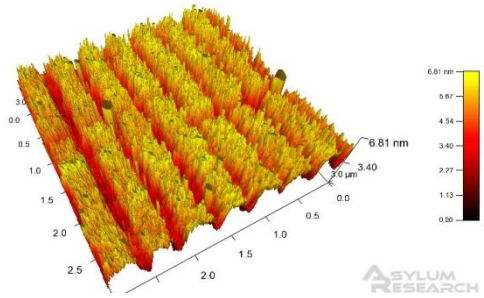

Figure A2: (SiO_2 Waveguide 5110-3) Washed with chromosulfuric acid. Image created on ArGyle Software, and optimized. As seen, 3 x 3 µm by 6.81 nm height range.

It can be seen that the image on the left (*Figure A1*) is a much cleaner (albeit still relatively dirty) waveguide, and uniform peaks and valleys are seen. In *Figure A2*, peaks and valleys are also seen, but the uniformity appears to be reduced. This could be caused by surface adsorbates in the valleys, preventing a true depth calculation or by an actual decrease in waveguide depth. The difference in waveguide depth can be seen more clearly in *Figures A3 and A4*.

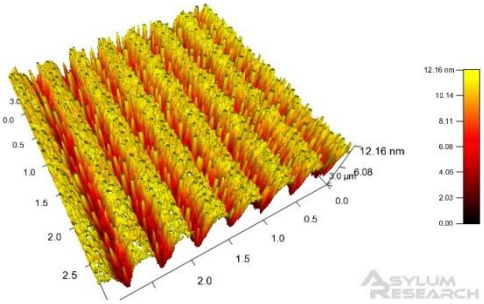

Figure A3: (SiO_2 Waveguide 5109-4) Washed with chromosulfuric acid. Image created on ArGyle Software, and optimized. As seen, 3 x 3 µm by 12.16 nm height range.

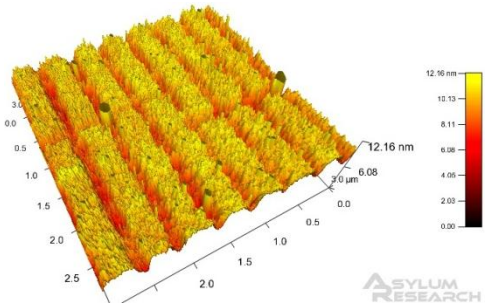

Figure A4: (SiO_2 Waveguide 5110-3) Washed with chromosulfuric acid. Image created on ArGyle Software, and made to compare to the 5109-4 waveguide. As seen, 3 x 3 µm by 12.16 nm height range.

Figures A3 and A4 indicate the differences between the two waveguide surfaces while reducing the impact of the imaging software. In both images 7 full peaks are visible, however the depth of the valleys in the waveguide in *Figure A4* is visibly smaller. .

Figures A5 and A6 further indicate the potential differences between waveguide 5109-4 and 5110-3.

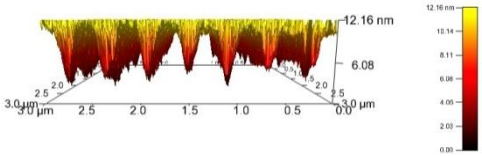

Figure A5: (SiO_2 Waveguide 5109-4) Washed with chromosulfuric acid. Image created on ArGyle Software. Head on view for valley comparison between waveguides. Height range is 12.16 nm.

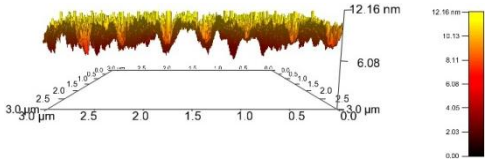

Figure A6: (SiO_2 Waveguide 5110-3) Washed with chromosulfuric acid. Image created on ArGyle Software. Head on view for valley comparison between waveguides. Height range is 12.16 nm.

Note that the *Figures A5 and A6* have been "z-clipped" to cut off artifacts or adsorbates that extend beyond the apparent peaks of the waveguides. When viewing *Figure A6* it is clear the surfaces is less "clean" than that of *Figure A5*, however specifically why the valleys appear more shallow remains unclear.

Figures A7 and A8 are the common waveguide views used for presentation and publication purposes.

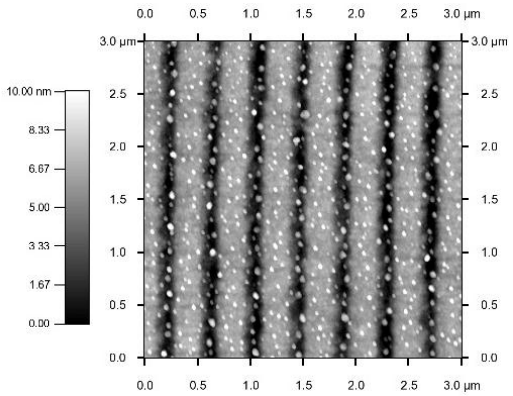

Figure A7: (SiO_2 Waveguide 5109-4) Washed with chromosulfuric acid. Image created on ArGyle Software. Flattened view commonly shown in articles and presentations. Separate and distinct particulate on the surface of the waveguide are clearly indicated.

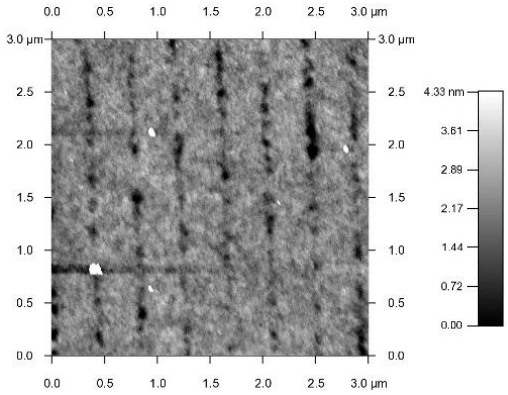

Figure A8: (SiO_2 Waveguide 5110-3) Washed with chromosulfuric acid. Image created on ArGyle Software. Flattened view. Although the surface looks cleaner than that in *Figure A7*, it is suspected that it is actually much more uniformly dirty, indicated by the mottling effect seen throughout the image when compared to *Figure A7*.

The ranges chosen in *Figures A7 and A8* are arbitrary, and relate only to image contrast. As discussed in the captions, it is suspected that while *Figure A8* appears to show a cleaner surface, it is actually more uniformly dirty (refer to *Figures A1-A6)*. The only conclusion that can be drawn from *Figures A1-A8* is that waveguide 5110-3 is dirtier than 5109-4. This could be a problem with the cleaning method, or an unavoidable problem of cleanliness variation between waveguides. Little, if anything about the variance in the depth of these waveguides can be concluded.

Figures A9-A16 are a continuation of the same waveguides used in *Figures A1-A8* (odd figures are 5109-4 and even figures are 5110-3) with the addition of an overnight soak in either HPLC H_2O (5109-4) or 1.5 N NaOH (5110-3).

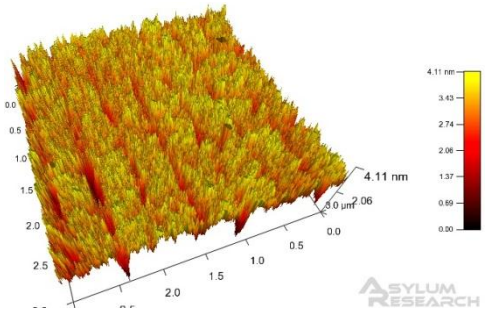

Figure A9: (SiO_2 Waveguide 5109-4) Overnight HPLC H_2O soak. Image created on ArGyle Software, and optimized.

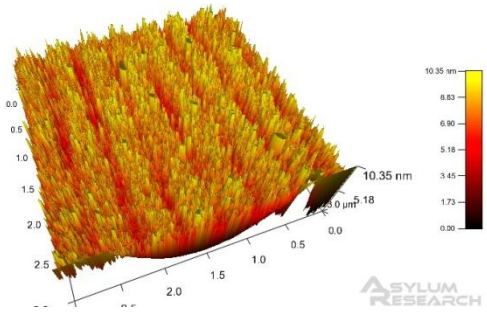

Figure A10: (SiO_2 Waveguide 5110-3) Overnight 1.5 N NaOH soak. Image created on ArGyle Software, and optimized.

It seems from *Figures A9 and A10* that the overall surfaces are not clean. Interestingly, the surface which seemed cleaner in the previous treatment (5109-4) is now the dirtier of the two. This could possibly be explained by "cleaning" from soaking 5110-3 in a strong base overnight. The artifact seen at the bottom of the image in *Figure A10* is an instrument, not a surface artifact.

In *Figures A11 and A12* it is clear to see waveguide 5109-4 (left) is much less clean than waveguide 5100-3 (right).

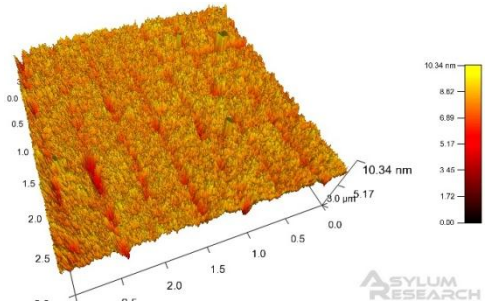

Figure A11: (SiO_2 Waveguide 5109-4) Overnight HPLC H_2O soak. Image created on ArGyle Software, and made to look compare with waveguide 5110-3. As seen the height range is set to 10.34 nm.

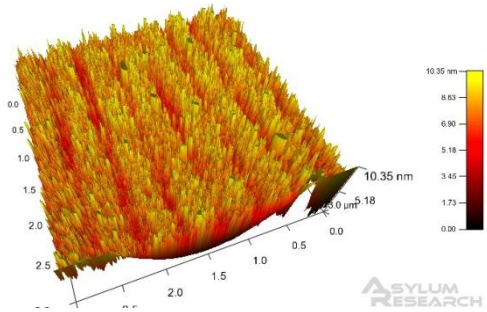

Figure A12: (SiO_2 Waveguide 5110-3) Overnight 1.5 N NaOH soak. Image created on ArGyle Software, and optimized. Height range is set at 10.34 nm.

It is very unlikely that an overnight soak in water would reduce the quality of a waveguide (i.e. etch the waveguide in some way). It is suspected that something is interfering with the AFM instrument's ability to detect the valleys present in the waveguide. This hypothesis needs to be explored further.

In *Figures A13 and A14*, direct comparison between the waveguides was not be made because the height ranges are different values. However, it appears that when comparing waveguide 5110-3 to itself before the overnight NaOH soak, NaOH does not etch the surface appreciably.

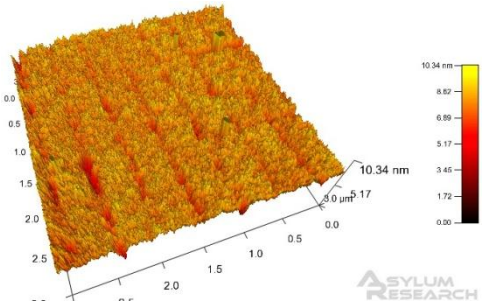

Figure A13: (SiO_2 Waveguide 5109-4) Overnight HPLC H_2O soak. Image created on ArGyle Software, head on view.

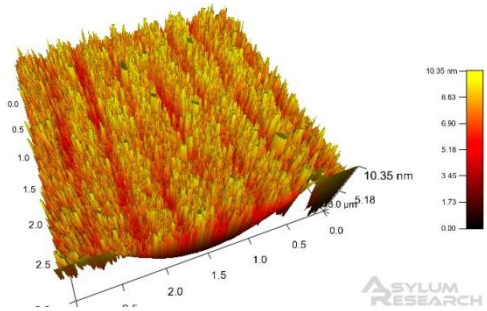

Figure A14: (SiO_2 Waveguide 5110-3) Overnight 1.5 N NaOH soak. Image created on ArGyle Software, head on view. Comparison with waveguide 5109-4 is difficult because of the variance in height range.

Figures A15 and A16 are the common waveguide views used for presentation and publication purposes.

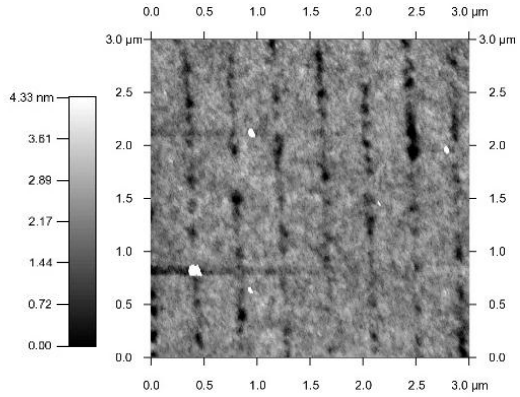

Figure A15: (SiO_2 Waveguide 5109-4) Overnight HPLC H_2O soak. Image created on ArGyle Software, flattened image and arbitrary height range.

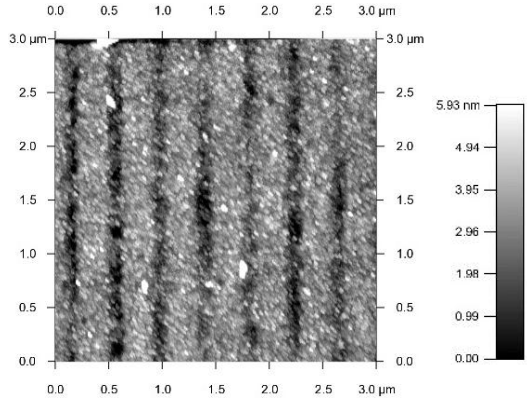

Figure A16: (SiO_2 Waveguide 5110-3) Overnight 1.5 N NaOH soak. Image created on ArGyle Software, flattened image and arbitrary height range.

The ranges chosen in the figures are arbitrary, and relate only to image contrast. As discussed in *Figures A7 and A8*, while *Figure A13* seems to show a cleaner surface, it is probably more uniformly dirty.

Variation in surface morphology between waveguides cannot be answered conclusively without more information. However, based on the images presented, NaOH does not appear to noticeably alter the waveguide surface and is a potential buffer for OWLS analysis.

University Honors College Copyright Release Form

We are planning to release this Honors Thesis in one or more electronic forms. I grant the right to publish **my thesis / my abstract (circle one)** entitled,
Molecular origins of peptide entrapment within polyethylene oxide brush layers
in the Honors College OSU Library's Digital Repository (D-Space), and its employees the nonexclusive license to archive and make accessible, under conditions specified below.

The right extends to any format in which this publication may appear, including but not limited to print and electronic formats. Electronic formats include but are not limited to various computer platforms, application data formats, and subsets of this publication.

I, as the Author, retain all other rights to my thesis, including the right to republish my thesis all or in part in other publications.

I certify that all aspects of my thesis which may be derivative have been properly cited, and I have not plagiarized anyone else's work. I further certify that I have proper permission to use any cited work which is included in my thesis which exceed the Fair Use Clause of the United States Copyright Law, such as graphs or photographs borrowed from other articles or persons.

Signature:_____

Printed Name:_____

Date: _____